SPECTRAL ANALYSIS OF EO-1 HYPERION DATA FOR SNOW GRAIN SIZE MAPPING IN A PART OF HIMALAYAN REGION

Arnab Saha[1*], Ankur Rana[1], Pradeep K. Garg[2] & Prafull Singh[3]

[1]Research Fellow, Uttarakhand Technical University, Dehradun, Uttarakhand, India,
Email: arnab.dd@gmail.com[*], ranaankur1991@gmail.com
[2]Professor, Uttarakhand Technical University, Dehradun, Uttarakhand, India,
Email: pkgiitr@gmail.com
[3]Asst. Professor, Amity University, Noida, Uttar Pradesh, India,
Email: psingh17@amity.edu

KEY WORDS: Spectral, Hyperion, Snow, Grain Size, NDSI

ABSTRACT: Snow is the part of atmosphere in the climate system of the Earth, and its physical parameters play an important role in hydrological and climate models. The present study concerns with the imaging spectroscopy to produce the snow cover maps and to estimate snow grain size in the North-Western Himalayan region. It is necessary to develop an approach to accurately map the snow cover, snow grain size spatially using advance remote sensing data and technique. Remote sensing techniques can provide spatial and temporal information of a large extent, economically and efficiently. In the present study, one of the important snow physical parameters (i.e., snow grain size) has been estimated using Spectral Angle Mapper (SAM) classification method and Grain Index (GI) method. The study has been carried out by using Hyperspectral EO-1 Hyperion sensor data of 12th January and 23rd January, 2016 to map the grain size of snow. The FLAASH (Fast Line-of-sight Atmospheric Analysis of Spectral Hypercubes) atmospheric correction model has been used to apply atmospheric correction from satellite images. The spectral reflectance of different types of snow grain size has been collected in the Hyperion image using spectral library. The important wavelengths are found for the retrieval of snow parameters, such as grain size. The snow cover maps were produced using Normalized Difference Snow Index (NDSI) technique. The snow maps were generated for dry snow, small grain size snow, medium grain size snow, large grain size snow and wet snow classes. This study is important for mapping of snow-cover characteristics which can provide valuable input for climatology, hydrology, and mountain hazard applications.

1. INTRODUCTION

"Remote sensing is the science and art of obtaining information about an object, area, or phenomenon through the analysis of data acquired by a device that is not in contact with the object, area, or phenomenon under investigation" (Lillesand *et al.,* 1999). A significant advantages of remote sensing are its ability to acquire information in inaccessible regions. Visible and infrared regions of the EMR spectrum are utilized in passive remote sensing, may be multispectral or hyperspectral remote sensing. Snow is an important subject of environment science and is a very useful environmental indicator of global changes in terms of long-term monitoring (Rinne *et al.,* 2009; Zhao *et al.,* 2013). The continuously changing the global climate and environment makes it necessary to realize and compute various hydrological components in competent water resource management for future prediction (Saha *et al.,* 2017). The temporal and spatial distribution of snow cover is an important indicator of the climate (Kropacek *et al.,* 2010; Zhao *et al.,* 2013). As one of the optical characteristics of snow and snow grain size are an important factor causing albedo changes and those is also one of the factors affecting in the global radiation balance (Zhao *et al.,* 2013). Hyperspectral sensors developed in 1980's by scientists at the Jet Propulsion Laboratories (JPL). These instruments can captured data in narrow contiguous wavelength bands. The spectral plots gives us fine details of the absorption phenomenon also. This was considered as a major development in the field of remote sensing. Hyperspectral imagery has been used to detect and map a wide variety of materials having characteristic reflectance spectra. For example, hyperspectral images have been used by geologists for mineral mapping (Clark and Swayze, 1995), and to detect soil properties including moisture, organic content, and salinity (Ben-Dor *et al.,* 2001; Rekha *et al.,* 2012). Vegetation scientists have successfully used hyperspectral imagery to identify vegetation species (Ustin *et al.,* 2002; Goodenough *et al.,* 2004; Bachmann *et al.,* 2004; Duk *et al.,* 2014).

Snow is an important subject of cryosphere-environment science and is a useful environmental indicator of global changes in terms of long-term monitoring (Rinne *et al.,* 2009; Zhao *et al.*, 2013). The temporal and spatial distribution of snow cover is an important indicator of the climate (Kropacek *et al.,* 2010; Zhao *et al.*, 2013). The spectral region between 350 and 2500 nm is called the reflected part of the spectrum. The reflectance of snow cover results from contributions of different parameters, namely snow grain size, moisture, contamination, solar zenith angle, sensor and snow depth and cloud cover (Negi *et al.,* 2015; Negi *et al.*, 2010). Numerous studies have been performed by different researchers on the spectral properties of snow in the optical region (Negi *et al.,* 2015). Snow plays an important role in hydrological and climate model especially snowmelt runoff modeling (Wang *et al.*, 2014). However, the mapping of snow and its physical parameters is very difficult using field instruments due to rough terrain and harsh weather. Moreover, such instruments could provide only point information in this dynamic feature. In such a case, remote sensing technique can play vital key role as it provides high spatial and temporal information of earth and its features. The spectral nature of snow makes its unique feature relative to other common earth surface materials. Snow shows high reflectance in the visible wavelength region and low reflectance in the shortwave infrared (SWIR) region (Garg *et al.,* 2014; Doggett *et al.,* 2006).

1.1 RESEARCH OBJECTIVES

The main objectives of this research work are to evaluate snow grain size mapping using EO-1 Hyperion Hyperspectral remote sensing data. The sub-objectives of the present study are:

1) Bad bands removal from hyperspectral remote sensing data.
2) Bad column removal from hyperspectral remote sensing data.
3) Atmospheric correction of hyperspectral remote sensing data.
4) To separate snow with other classes
   – Using NDSI
   – Using Classification Technique (SAM)
5) To identify snow grain size
   – Using classification technique
   – Using grain size index

2. STUDY AREA

Dhundi areas of Himachal Pradesh, India have been selected for the present study. Himachal Pradesh is famous for its natural beauty, hill stations, and temples. Himachal Pradesh has been ranked fifteenth in the list of the highest per capita incomes of Indian states and union territories for year 2013-14. The state has several valleys and more than 90% of the population lives in rural areas (*Wikipedia- Himachal Pradesh*). The study area is located in north of greater Himalayan range (lies 32°21'13"N latitude and 77°7'47"E longitude) at Dhundi area of Himachal Pradesh, India. Rohtang Tunnel is a tunnel being built under the Rohtang Pass in the eastern Pir Panjal range of the Himalayas on the Leh-Manali Highway. Rohtang tunnel is not exactly under Rohtang pass; it is slightly west of the pass. The southern end (portal) of the tunnel is reached by turning left at Palchan, 10 km north of Manali on the way to Rohtang pass or about 40 km before Rohtang pass. After crossing Solang village, Dhundi is reached after 10 km. The south end of the tunnel is just north of Dhundi across the [[Bhaga River] Tributary of Chenab River]] (*Wikipedia- Rohtang Tunnel*). The climate of the Dhundi area resembles the cold climate of Himachal Pradesh in general but its northern position and its proximity to the hills give its own peculiarity. Though the region lies well outside the tropics yet its climate is like rest of the north India essentially because of Himalayan chain. The climate in Dhundi is warm and temperate. Dhundi has a significant amount of rainfall during the year. This is true even for the driest month. The average temperature in Dhundi is 9.4 °C. Precipitation here averages 1094 mm. The driest month is November, with 28 mm of rain. With an average of 156 mm, the most precipitation falls in March. June is the warmest month of the year. The temperature in June averages 16.9 °C. January has the lowest average temperature of the year. It is -1.0 °C. There is a difference of 128 mm of precipitation between the driest and wettest months. During the year, the average temperatures vary by 17.9 °C (Patel *et al.*, 2016).

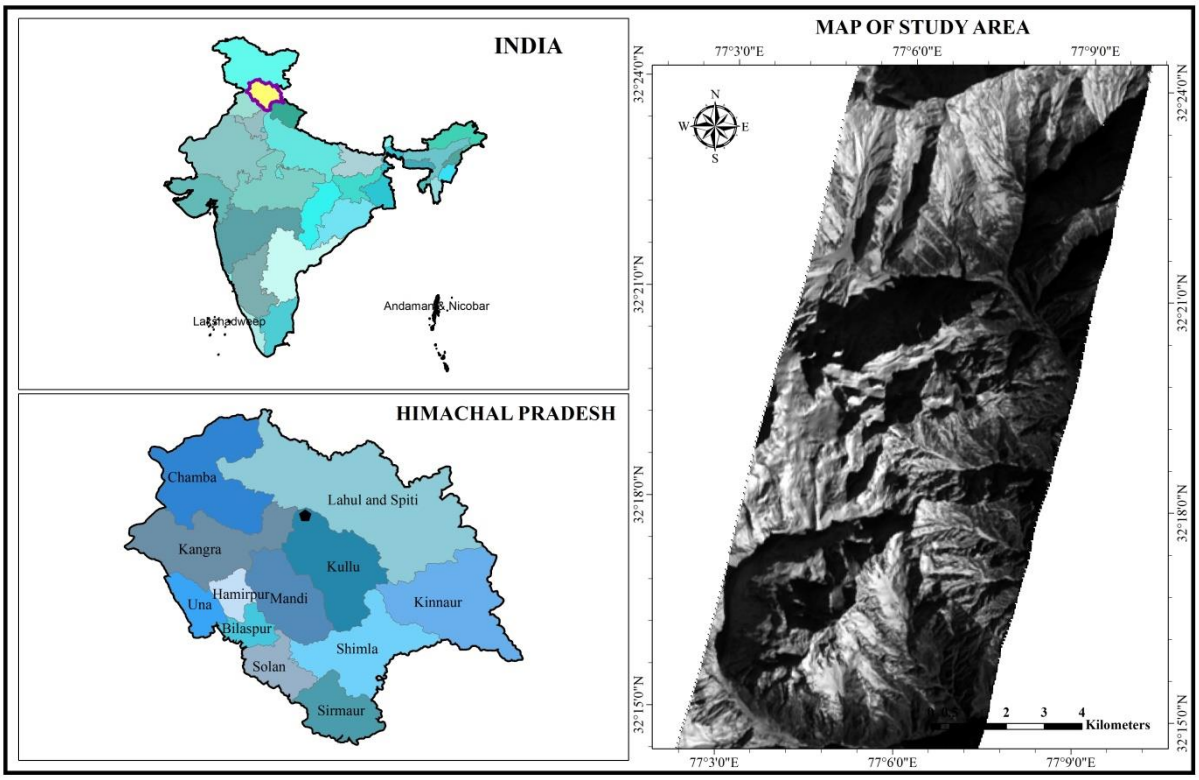

Figure 1: Study area map- Dhundi, Himachal Pradesh, India

3. MATERIALS AND DATA USED

Hyperion is an EO-1 (Earth Observation- 1) satellites sensor which was developed by NASA˝s new millennium program in 21st November, 2000, is the first spaceborne Hyperspectral sensor for Earth Observation studies (Pande *et al.*, 2009). Its orbits in an Earth sun-synchronous (polar) orbit at an altitude of 705 km. Hyperion sensor are a push broom imaging instrument with a high spectral resolution (Tatsumi *et al.*, 2010). Each image captures the spectrum of a line 30 m along track and 7.5 km wide perpendicular to the satellite motion (Cavalli *et al.*, 2008) and covers an area of 7.7x100 square km per image with high radiometric accuracy (12 bit quantization) (*Encyclopedia of Earth Sciences Series, 2014*). There are 220 unique bands with spectral range of 357 - 2576 nm at 10 nm band width. The Level 1 radiometric product has total 242 bands but only 198 bands are calibrated (band 8 to 57 for VNIR region and 77 to 224 in SWIR region) (Datt *et al.*, 2003; Li *et al.*, 2009). Because of an overlap between focal planes of VNIR and SWIR, there are only 196 unique channels (Mitran *et al.*, 2015). Visible and near Infrared region (VNIR) i.e. 0.4 to 1µm having 70 bands and the other operates in Shortwave Infrared region (SWIR) i.e. 0.9 to 2.5µm having 172 bands. The reason for not calibrating all 242 channels is low detector responsively. The data in the form of cubes is put into Hierarchical Data Format (HDF) format and is archived. The dataset used for current analysis is radiometrically corrected Hyperion L1R radiance dataset.

Table 1: Specification of EO-1 Hyperion

Sensor altitude	705 kms	No. of rows	256
Spatial resolution	30 meters	No. of columns	3128
Radiometric resolution	16 bits	VNIR range	0.45 - 1.35
Swath	7.2 kms	SWIR range	1.40 - 2.48
IFOV (mrad)	0.043		

The Hyperion image over Dhundi region, Himachal Pradesh was acquired on 12th January, 2016 at 03:36:14 AM and 23rd January, 2016 at 03:39:45 AM. The dimensions of the acquired dataset are 256 (ground samples of 30m width) x 3407 (lines) x 242 (bands). The first data is acquired in a wavelength range to 355.5900 nm to 2577.0801 nm at approximately 10nm sampling interval and the signal to noise ratio is 65 – 130 dB and the second data is acquired in a wavelength range to 355.5900 nm to 2577.0801 nm as same as first data (Pargal *et al.*, 2011).

4. METHODOLOGY

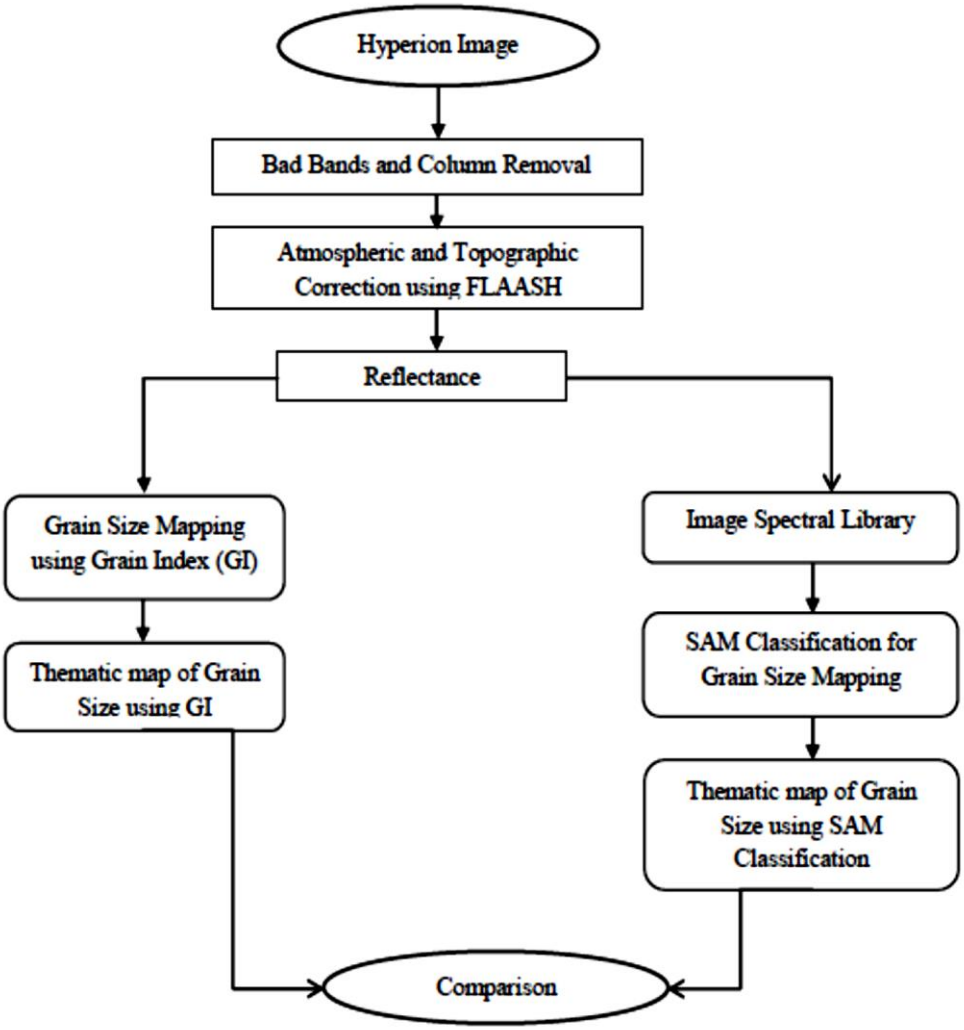

Figure 2: Methodology flowchart

Processing of high dimensional hyperspectral data is a very challenging task and the computational complexity is a result of vast data volume in numerous spectral bands. Since Hyperion sensor operates from a space platform with modest surface signal levels and a full column of atmosphere attenuating the signal, the data demand careful processing to manage sensor noise (Rama Rao *et al.*, 2007). The errors are said to be caused due to calibration differences in the detector array (Goodenough *et al.*, 2003). The Hyperion datasets has more error when it was collected and then, it will be corrected for bad bands, bad columns and atmospheric correction process. Preprocessing of hyperspectral images is required not only for removing sensor errors during acquisition but also for display, band selection and to reduce computational complexity. The following section discusses briefly about pre-processing steps carried out and atmospheric correction done on Hyperion dataset.

4.1 Satellite Data Processing

The Hyperion data was initially processed by the EO-1 satellite product generation system (EPGS) and distributed at different processing levels (Singh and Singh, 2015). In this present study the radiometrically corrected level 1R data, which became effective from January 2017, has been used. The level 0 (raw) datasets were corrected for dark current (remove residual charge in the detectors), sensor bias effects and two specific artifacts known to affect the

SWIR region to produce level1R product: (1) SWIR smearing, which is the leakage of signal from one pixel into the next readout pixel in the spectral direction, and (2) SWIR echo, which occurs when the signal from one image echos into a later pixel (Beiso *et al.*, 2002). The data are available in 16-bit signed-integer radiance values. Level 1R data are used for FLAASH atmospheric correction in ENVI image processing software. Hyperion tools is installed in ENVI software for first level image processing. Its converted the raw data in a L1R data. FLAASH allows us to define all parameters that influence atmospheric absorption and scattering, such as relative solar position, aerosol and scattering models, visibility parameters, ozone total vertical column, adjacency effects (for flat areas only), and artefact suppression, and obtain water vapour data (Garcia-Torres *et al.*, 2014; Negi *et al.*, 2011).

To estimate signal-to-noise ratio of Hyperion datasets used in the present study homogeneous area method is used (Smith and Curran, 1998). The method is widely used and employed to make a quick estimate SNR. Based on variability of landcover small window of 2×2 and 4×4 sizes were used to estimate signal. Homogeneous areas were visually selected in vegetation, water and barren land. The method is widely used and employed to make a quick estimate SNR. Based on variability of landcover small window of 2×2 and 4×4 sizes were used to estimate signal. Homogeneous areas were visually selected in vegetation, water and barren land. The signal (Ra) was estimated for each landcover by averaging the pixel responses in the window used. The noise (Rsd) component was estimated by standard deviation of the pixel response within the window (Kang *et al.*, 2015).

4.1.1 Identification and Balancing of Bad Columns:

In a pushbroom sensor, a poorly calibrated detector detecting an image on VNIR or SWIR arrays leaves high frequency errors ("vertical stripes") on the image bands (Aggarwal and Garg, 2015). In the present study a tool was used to compensate for the striping by visually identifying bad columns and develop a filter to balancing for the bad columns. Hyperion datasets global and local de-striping approaches have been suggested in the order to compensate for striping. In this study, more bad columns are identify in VNIR and SWIR bands. It was visually identified avoid enforcing severe change in the spectra. A total of 120 bands were collected from the first data of 12th January, 2016. A total of 43 bad columns were identified in 6 VNIR bands and 20 SWIR bands of Dhundi region dataset. A total of 138 bands were collected from the second data of 23rd January, 2016. A total of 25 bad columns were identified in 4 VNIR bands and 8 SWIR bands of second Dhundi region dataset.

A bad column removal filter was generated to target the removal of bad columns in each band. Without taking into account the bad column value the 3×3 neighborhood mean was worked for the replacing of the bad columns (Kumar and Garg, 2012). The average value of the neighbor rows are taken in order to implement this a 3×3 filter was designed (Figure 3-3) with positional values as (-1,1) =1, (1,0) =1, (-1,-1) =1, (0,1) =0, (0,0) =0, (0,-1) =0, (1,1) =1, (1,0) =1 and (1,-1) =1. The filter runs on the bands identified as containing bad columns. The user interface allows the user to enter the band numbers that contain bad columns and column number of the specified band.

4.2 Preparation of Input Data and Selection criterion

The input parameters required for FLAASH are to be computed before the image is subjected to atmospheric correction (Kumar *et al.*, 2017). Sensor type, Pixel size, Ground elevation, Solar zenith angle, Flight data and time, Scene centre latitude and longitude, Sensor altitude, Visibility, Atmospheric model, Aerosol model, Water retrieval, Adjacency range and zone, Reflectance scale factor and additional parameters are required from the user to run the FLAASH model successfully is sensor specific and specific to ground situation. Selection of the input parameters has a direct bearing on the output of the atmospheric correction models.

To calculate the nominal parameters related to the orbital inclination of the satellite, the sensor geometry on the surface, the radius of the orbit and its angular velocity some earth surface parameters are required. The calculation method is simply a function of the latitude and longitude. The satellite information is computed assuming the orbit is circular but that the earth is a spheroid. The results are approximate but are useful to provide starting choices in atmospheric correction models (Jupp *et al.*, 2004).

In Visibility field, enter an estimate of the scene visibility in kilometers. The initial visibility value is assumed for the atmospheric correction if the aerosol is not being retrieved. The following range gives the approximate scene visibility values based on weather conditions: in clear weather condition scene visibility is 40-100 km, in moderate haze weather condition scene visibility is 20-30 km and thick haze weather condition scene visibility is 15 km or less.

Based on geographic location the user has to choose the correct atmospheric model for the correction. FLAASH have six atmosphere types based on a seasonal-latitude surface temperature MODTRAN modelled atmospheres. Select a model whose standard column water vapor amount is similar to, or somewhat greater than, that expected for the scene.

Aerosol model supports four basic aerosol types: rural, urban, maritime, and tropospheric. Based on the geographic location the user has to make a choice. FLAASH include a method for retrieving the water amount for each pixel. To solve the radiative transfer equations that allow apparent surface reflectance to be computed, the column water vapor amount for each pixel in the image must be determined. FLAASH includes a method for retrieving the water amount for each pixel.

FLAASH allows adjacency range of 0.5 to 1 km. As the two dated dataset in use belong to a heterogeneous area an adjacency range of 0.5 km is selected with weight factor of 1. Three multiscatter models are available in FLAASH Isaacs, Scaled DISORT, and DISORT. The recommended Scaled DISORT with 8 streams (signifying 8 directional adjacency) is selected for the present study (Kawishwar *et al.*, 2007). More optional parameters available in FLAASH are aerosol scale height, CO_2 mixing ratio, modtran resolution, zenith angle and azimuth angle. The scene of the study area is not seen to be affected by aerosol scale height and CO_2 mixing ratio, these options were not utilized during atmospheric correction.

4.3 Snow Grain Size Measurement

Snow grain size measured in two ways. The most analytical, but time-consuming, technique is by stereology (Dozier *et al.*, 1987; Nolin and Dozier, 2000). The two techniques have been applied to map snow grain size: Spectral Angle Mapper (SAM) and Grain Size Index (GI) method proposed based on the field collected hyperspectral reflectance data (Negi *et al.*, 2010).

4.3.1 Grain Size mapping using GI:

The snow grain size mapping was calculating using the grain index method and used by based on the field-collected Hyperspectral reflectance data (Negi *et al.*, 2010). In the present study, the Hyperion band number 24 (central wavelength 589.62 nm) and band number 90 (central wavelength 1043.59 nm) were used for both dataset. The snow map generating of fine, medium, and coarse grain size classes. It was generated using the threshold grain index values. To be sure that the index shows snow grain size, one should use a snow classification algorithm in addition to check if there really is snow on the ground.

$$\text{Grain index} = \frac{\text{Reflectance (590 nm)} - \text{Reflectance (1050 nm)}}{\text{Reflectance (590 nm)} + \text{Reflectance (1050 nm)}}.$$

4.3.2 Grain Size mapping using NDSI:

Before estimated the snow grain size, it had to extract the sow cover area, which requires the difference between snow cover surface and non-snow cover surface. Currently, there are five main methods to extract snow cover using remote sensing data. They are visual interpretation, a multiband imagery calculation, the brightness-threshold method, a snow cover index, and a radiative transfer model (Zhao *et al.*, 2013). The above relation was only valid for snow cover pixels, which were selected with the help of normalized difference snow index (NDSI) and visible channel reflectance.

$$\text{NDSI} = \frac{\text{Reflectance (Green)} - \text{Reflectance (SWIR)}}{\text{Reflectance (Green)} + \text{Reflectance (SWIR)}}.$$

In this present study, the Hyperion band number 15 (central wavelength 498.04 nm) and band number 146 (central wavelength 1608.61 nm) were used for both dataset. Therefore Normalized Difference Snow Index (NDSI) was applied on Hyperion scenes (Negi *et al.*, 2010).

$$\text{Grain Index (Hyperion)} = \frac{\text{Ref (24)} - \text{Ref (90)}}{\text{Ref (24)} + \text{Ref (90)}}$$

$$\text{NDSI(Hyperion)} = \frac{\text{Ref (15)} - \text{Ref (146)}}{\text{Ref (15)} + \text{Ref (146)}}$$

4.3.3 Grain Size mapping using SAM:

SAM (Spectral Angle Mapper) a supervised classification method, is used to calculate the grain size. The SAM method obtain the similarity between the two spectra (i.e. the pixel spectra to known/reference spectra) measured by an angle between two vectors representing these spectra. A Hyperion image of upper portion of Himalaya was selected for snow grain size estimation as this area is mostly glaciated with gradual slopes (less than 5^{o}) and to avoid fractional snow cover. In this classification, collects the spectra from the image and identify the each separate class. Then this separate spectra of separate class was stored in a spectral library. The selected image spectra were further used as reference spectra for mapping grain size using the SAM method (Rowan and Mars, 2003). The extracted endmembers spectra are then compared with the in-situ measured spectral reflectance using optical spectro-radiometer for identification (Singh *et al.*, 2015). The selected image spectra endmembers were further used as reference spectra for mapping grain size using SAM method.

5. RESULTS

5.1 Hyperion Data Processing

The Hyperion sensor instrument provides a new class of Earth observation data for improved Earth surface characterization (Silverman *et al.*, 2000). Hyperion has 242 bands but provides a high resolution hyperspectral imagery capable of 220 spectral bands (from 0.4 to 2.5 µm) with a 30-meter resolution. There are a number of corrupted pixels and dark black vertical stripes in the Hyperion imagery datasets that are caused by calibration differences in Hyperion detector array and temporal variations in the detector's response (Acito *et al.*, 2011). Detection of bad columns is carried out using set thresholds based on median values from its neighborhood. Bad columns are removed by neighbor's pixel average value in spatial pixel editor approach. There are many bad columns and bad pixel in Hyperion imagery dataset. The bad columns or bad pixel have zero DN value for calibration differences in Hyperion detector array. This DN values are change by neighbors average pixel values in imagery. The figures below show examples of different types of bad pixels in the Hyperion data.

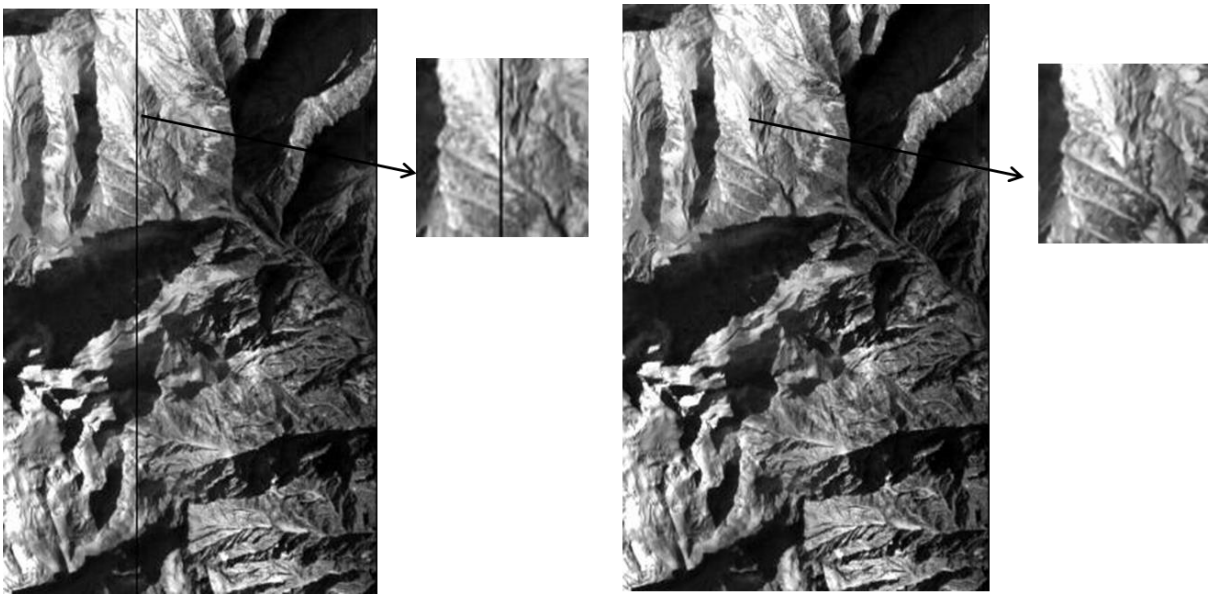

Figure 3: Bad column correction using Hyperion tools in Band 94, 12th Jan, 2016 data

5.2 Atmospheric Correction using FLAASH

After the removal of the bad bands, bad columns and destriping the resized 120 bands in 12th January, 2016 dataset and 138 bands in 23rd January, 2016 dataset were corrected for atmospheric errors using the FLAASH (Fast Line-of-Sight Atmospheric Analysis of the Spectral Hypercubes) model of ENVI's atmospheric correction model. The Hyperion image of Dhundi area is badly effected by atmospheric condition such as haze and its time of acquisition. Visible, infrared and short wave infrared can be corrected for atmospheric errors using FLAASH atmospheric correction model (Aggarwal and Garg, 2015). The spectra of snow is calculated from radiative transfer model, positioning for scattering and absorption by the snow grains, water absorption, and particulates. Spectroradiometer was used to measuring spectra of different snow and mixed of other feature snow-covered land surface objects. The

raw image of Hyperion is not used for measuring a snow spectra. After that FLAASH run, it's used to measuring for snow spectral signature. Before the FLAASH run, the images of snow spectra shows wrong spectral signature and its showing a different spectra of each feature of the image. Snow mixed objects spectra is also differ in that process. The figure below shows the difference between initial image of Hyperion and after the running of FLAASH image's snow spectra.

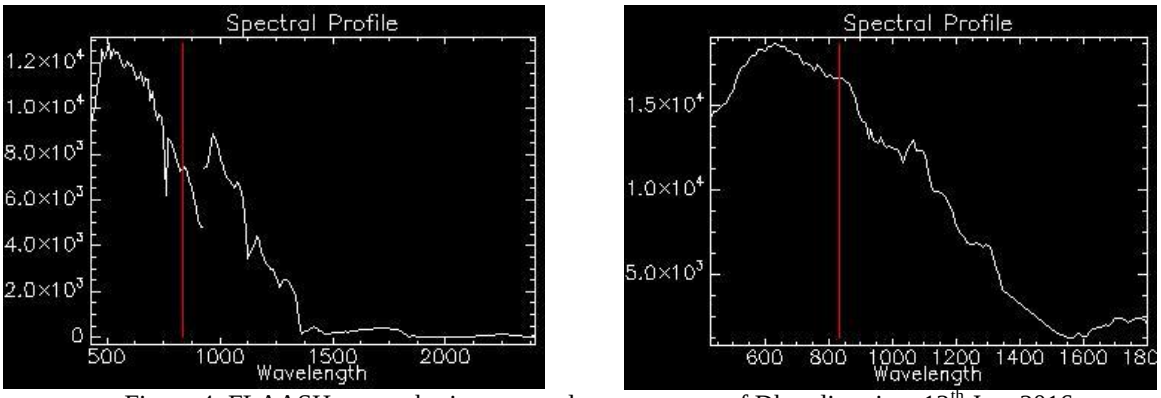

Figure 4: FLAASH atmospheric corrected snow spectra of Dhundi region, 12th Jan, 2016

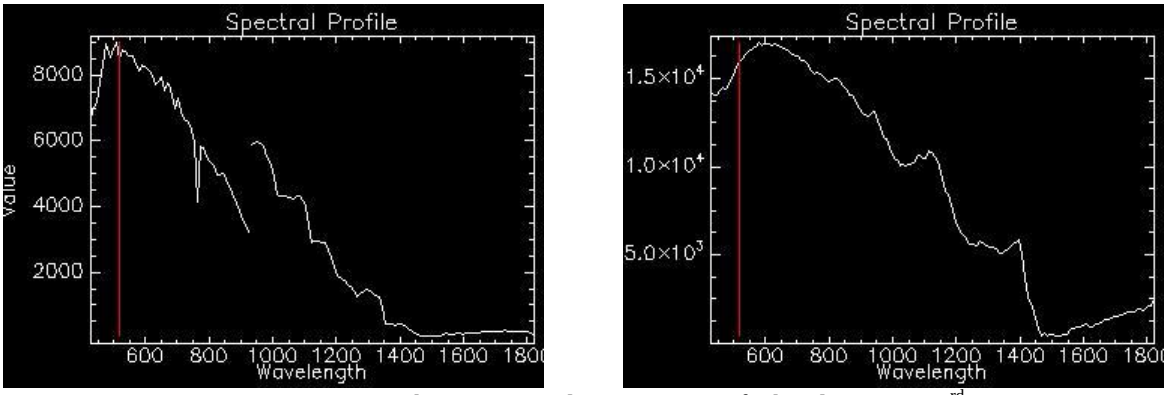

Figure 5: FLAASH atmospheric corrected snow spectra of Dhundi region, 23rd Jan, 2016

5.3 Snow Grain Size Mapping

5.3.1 Snow Grain size mapping using GI:

The snow grain size mapping was calculated using the grain index method and it was used by based on the collected Hyperspectral reflectance data. In the present study, the Hyperion band number 24 (central wavelength 589.62 nm) and band number 90 (central wavelength 1043.59 nm) were used for both dataset. The snow map generating for dry snow, small grain size snow, medium grain size snow, large grain size snow and wet snow classes. Before estimated the snow grain size, it had to extract the sow cover area, which requires the difference between snow cover surface and non-snow cover surface. The formula was used for calculating GI and NDSI for snow grain size mapping. Both of the datasets were calculated for GI mapping. The snow mask was also generated for both of the images. The figure below shows the spectral distribution of the snow grain sizes for two datasets.

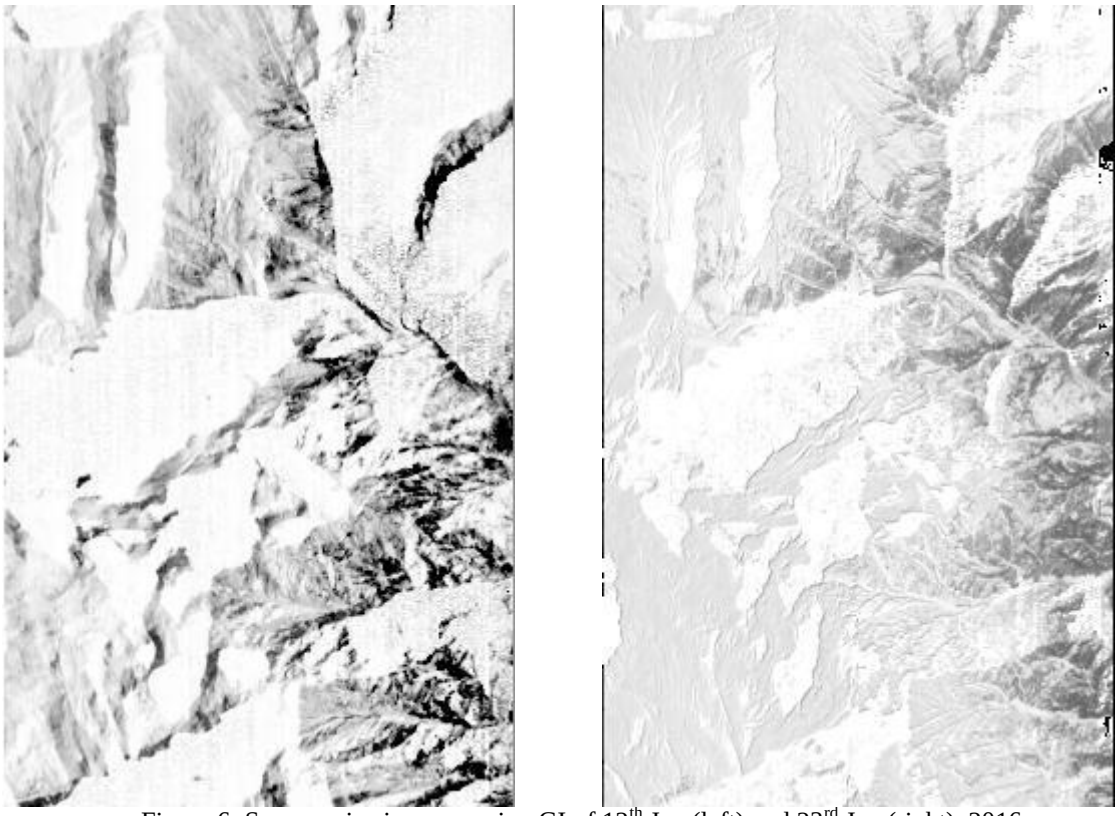

Figure 6: Snow grain size map using GI of 12th Jan (left) and 23rd Jan (right), 2016

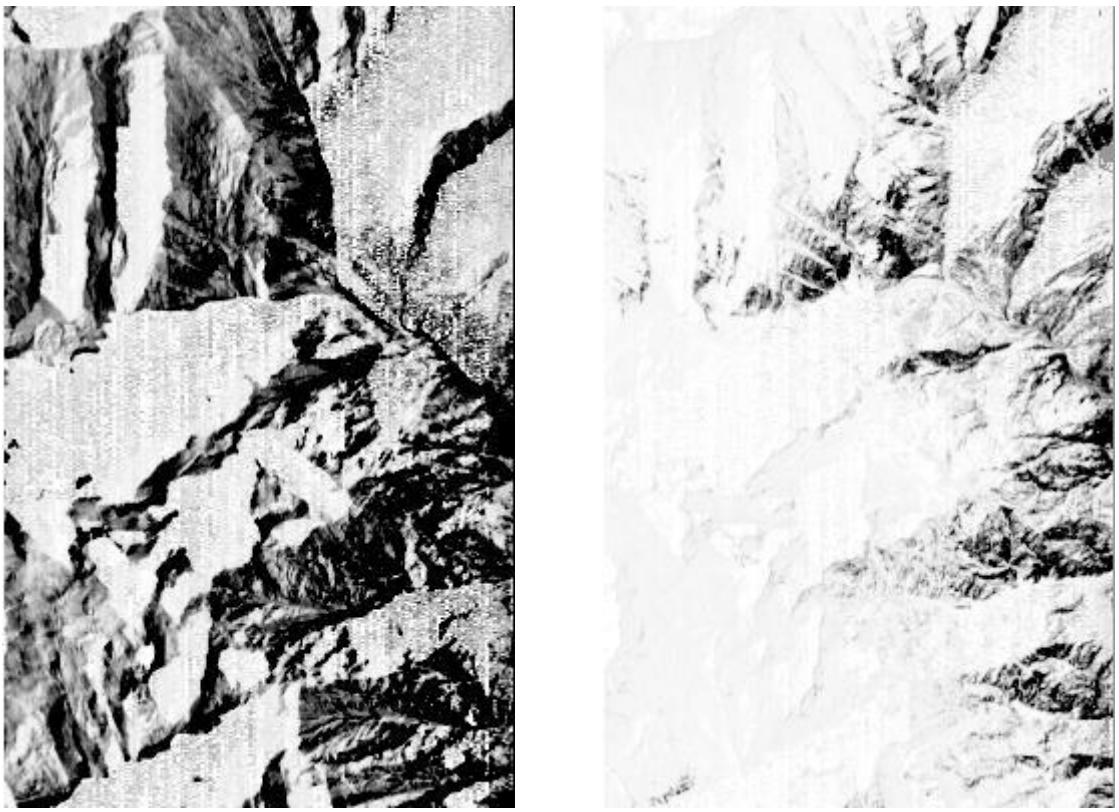

Figure 7: NDSI derived using Hyperion data of 12th Jan (left) and 23rd Jan (right), 2016

Snow grain size map was estimated using snow grain size index for a small part of the greater Himalaya range on 12th January and 23rd January, 2016. On the comparison between two dataset image of GI method classified image shows that 7.55% area is increased in fine grain size snow, 4.96% area is decreased in medium grain size snow and 3.48% area is also decreased in coarse grain size snow. Unclassified areas are showing in images which are in black color (fig.6 and fig.7). But in comparison image of GI method classified image shows that 3.11% area is decreased in 12th January dataset image.

Table 2: Comparison of Snow grain size using GI classified image

Snow grain size (mm)	**GI method (% area) of 12th Jan, 2016**	**GI method (% area) of 23rd Jan, 2016**
Fine (0.0-0.25)	7.89	15.44
Medium (0.25-0.50)	22.64	17.68
Coarse (0.50-0.83)	11.96	8.48
Unclassified	57.51	54.40

5.3.2 Snow Grain size mapping using SAM:

The SAM classification has been done using the spectral library approach. The different spectra was collected from reflectance image of Hyperion and the collected spectra was save in spectral library for SAM classification. An image spectra has been generated for dry snow, small grain size snow, medium grain size snow, large grain size snow and wet snow using simple z-profiling in ENVI software. In this classification, collects the spectra from the image and identify the each separate class. In this classification method, some area was not classified because of low spectral signature. So, this class was not classified and named by unclassified class in the image. This was happen for high altitude area, back side shadow of hilly region etc. The matrix, comparing different snow grain size classes using the results classification of the SAM methods, shows the overall classified area to be approximately 47% and the unclassified area was 53% approx. in 12th Jan, 2016 dataset. Another dataset define 36.28% classified and 63.72 % unclassified in 23rd Jan, 2016.

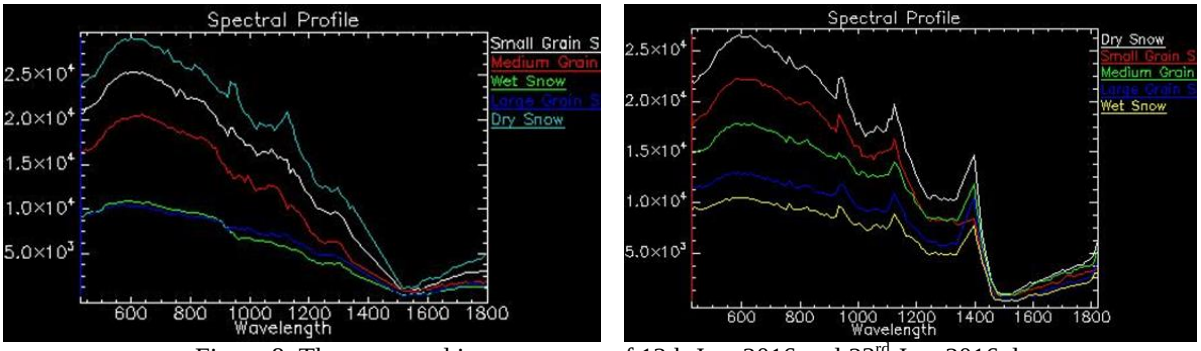

Figure 8: The generated image spectra of 12th Jan, 2016 and 23rd Jan, 2016 data

Snow grain size map was estimated using snow grain size index and compared with SAM classified image for a small part of the greater Himalaya range on 12th January and 23rd January, 2016. On comparison between two dataset of SAM classified image shows that 7.26% area is increased in small grain size snow cover area, 3.22% area is decreased in medium grain size snow and 3.88% area is also decreased in large grain size snow. The present methodology for the mapping is indicates of snow grain size mapping using SAM is well suited for Himalayan region at varying altitude from 4000 m and above.

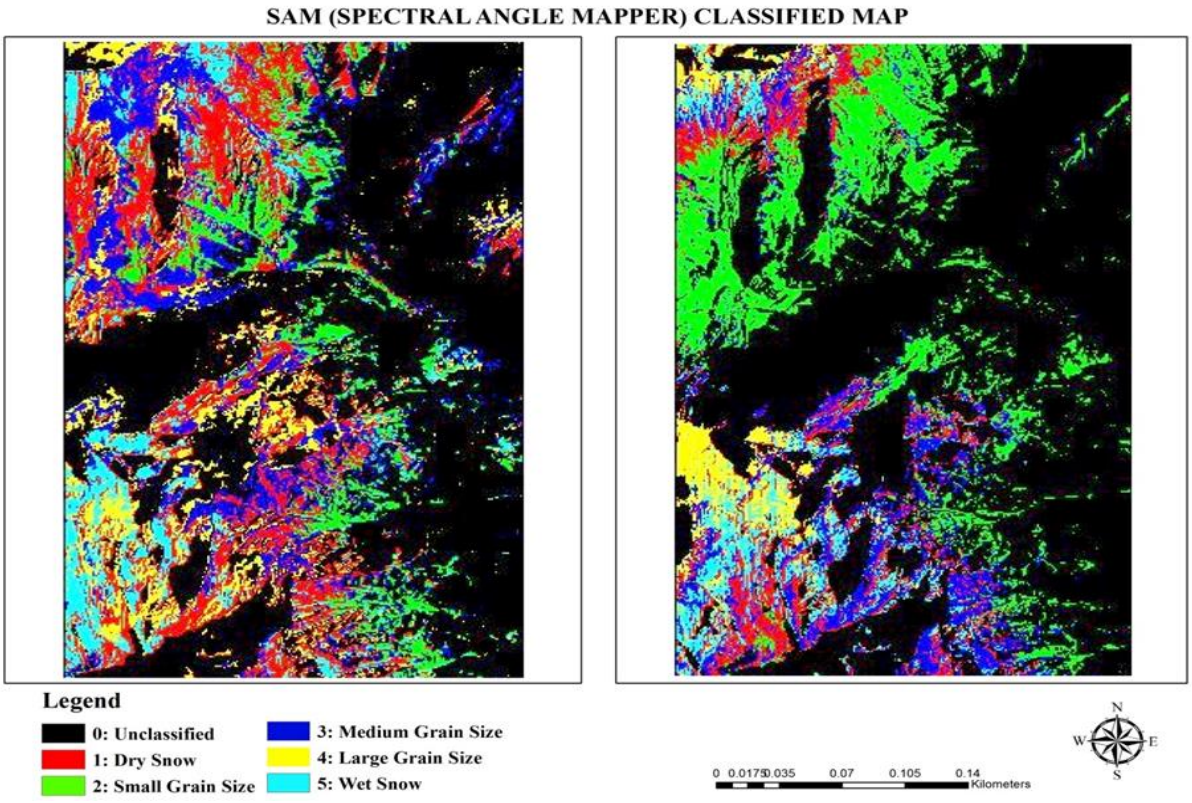

Figure 9: Spatial distribution of grain sizes at a continuous scale using SAM classification of 12th January (left side) and 23rd January (right side) imagery

Table 3: Comparison of Snow grain size using SAM classified image

Snow Grain Size Class	**SAM Classification method (% area) of 12th Jan, 2016**	**SAM Classification method (% area) of 23rd Jan, 2016**
Dry snow	15.92	7.33
Small grain size	6.38	13.64
Medium grain size	10.43	7.21
Large grain size	7.44	3.56
Wet snow	6.82	4.54
Unclassified	53.01	63.72

6. CONCLUSION

SAM and GI methods provides the properties of snow such as snow cover area snow grain size and temperature are very important for hydrological modeling. These classification techniques are very important when quantity of information is not necessary such as glacier forecasting, melting snow, climate study etc. For the analysis 30m spatial resolution EO1-hyperion data of 12th January and 23rd January, 2016 has been used. These methods of snow physical parameter measurements are very easy, otherwise its difficult and time consuming. In this study, both SAM and NDSI approaches can be used to map snow cover area. The analysis procedure consists of FLAASH (Fast Line-of-sight Atmospheric Analysis of Spectral Hypercubes) atmospheric correction model. The SAM method was found useful to identify the different levels of snow, since as per our knowledge. The GI method was also found to useful identity of snow but it's not a only suitable techniques for measurement of snow cover area. The wavelength near of 590 nm and 1040 nm are most sensitive to snow grain size. This wavelength consists in band 24 and band 90 of Hyperion imagery. Therefore, the future investment focus on more number of bands and radar image to measurement the snow cover area and snow grain size.

References

Acito, N., Diani, M. and Corsini, G., 2011. Subspace-based striping noise reduction in hyperspectral images. IEEE Transactions on Geoscience and Remote Sensing, 49(4), pp.1325-1342.

Aggarwal, A. and Garg, R.D., 2015. Systematic approach towards extracting endmember spectra from hyperspectral image using PPI and SMACC and its evaluation using spectral library. Applied Geomatics, 7(1), pp.37-48.

Bachmann, C. M., Ainsworth, T. L. and Fusina, R. A., 2004. Improvements to LandCover and Invasive Species Mapping from Hyperspectral Imagery In the Virginia Coast Reserve. IEEE Transactions on Geoscience and Remote Sensing, 36(4), pp. 4180 – 4183.

Beiso, D., 2002, October. Overview of Hyperion on-orbit instrument performance, stability, and artifacts. In Applied Imagery Pattern Recognition Workshop, 2002. Proceedings. 31st (pp. 95-101). IEEE.

Ben-Dor, E., Patinand, K., Banin, A. and Karnieli, A., 2001. Mapping of several soil properties using dais 7915 hyperspectral scanner data. A case study over clayey soils in Israel. International Journal of Remote Sensing, 12, pp. 500 520.

Cavalli, R.M., Fusilli, L., Pascucci, S., Pignatti, S. and Santini, F., 2008. "Hyperspectral Sensor Data Capability for Retrieving Complex Urban Land Cover in Comparison with Multispectral Data: Venice City Case Study (Italy)", Sensors, 8, pp. 3299-3320.

Clark, R. N. and Swayze, G. A., 1995. Mapping minerals, amorphous materials, environmental materials, vegetation, water, ice, snow and other materials: The USGS tricorder algorithm. Summaries of the Fifth Annual JPL Airborne Earth Science Workshop, JPL Publication, 1, pp. 39 40.

Datt, B., McVicar, T.R., Van Niel, T.G., Jupp, D.L.B. and Pearlman, J.S., 2003. Preprocessing EO-1 Hyperion hyperspectral data to support the application of agricultural indexes. IEEE Transactions on Geoscience and Remote Sensing, 41(6 Part 1), pp. 1246-1259.

Doggett, T., Greeley, R., Chien, S., Castano, R., Cichy, B., Davies, A.G., Rabideau, G., Sherwood, R., Tran, D., Baker, V. and Dohm, J., 2006. Autonomous detection of cryospheric change with hyperion on-board Earth Observing-1. Remote Sensing of Environment, 101(4), pp.447-462.

Dozier, J., Davis, R. E., and Perla, R., 1987, On the objective analysis of snow microstructure. In Avalanche Formation, Movement and Effects (B. Salm and H. Gubler, Eds.), IAHS Publication No. 162, Wallingford, UK, pp. 49–59.

Duk, J., Soon, S. and Bo, J., 2014. Use of Terrestrial Hyperspectral Sensors for Analyzing Spectral Reflectance Characteristics of Concrete. 한국측량학회지, 32(3), pp.185-190.

Encyclopedia of Earth Sciences Series, 2014.

Garcia-Torres, L., Caballero-Novella, J.J., Gomez-Candon, D. and De-Castro, A.I., 2014. Semi-automatic normalization of multitemporal remote images based on vegetative pseudo-invariant features. PloS one, 9(3), p.e91275.

Garg, V., Aggarwal, S.P., Thakur, P.K. and Nikam, B.R., 2014. Snow and its grain size mapping using Hyperspectral remote sensing data, ISPRS TC VIII, WG VIII/6 International Symposium on "Operational Remote Sensing Applications: Opportunities, Progress and Challenges".

Goodenough, G.D., Dyk, A., Niemann, O.K. and Pearlman, J.S., 2003. Preprocessing Hyperion and ALI for forest classification. IEEE Transactions on Geoscience and Remote Sensing, 41(6 Part 1), pp. 1321-1331.

Goodenough, D. G., Pearlman, J., Chen, H., Dyk, A., Han Tian., Li. J., Miller, J. and Niemann, 2004. K. O., Forest Information from Hyperspectral Sensing. IEEE Transactions on Geoscience and Remote Sensing, 36(4), pp. 2582–2589.

Jupp, D.L.B., Datt, B., Lovell, J., Campbell, S. and King, E., 2004. Backgroung notes for Hyperion data user workshop, CSIRO office of space science and applications, Earth Observation Centre.

Kang, W., Yu, S., Seo, D., Jeong, J. and Paik, J., 2015. Push-broom-type very high-resolution satellite sensor data correction using combined wavelet-fourier and multiscale non-local means filtering. Sensors, 15(9), pp.22826-22853.

Kawishwar, P., 2007, January. Atmospheric Correction Models for Retrievals of Calibrated Spectral Profiles from Hyperion EO-1 Data. ITC.

Kropacek, J., Feng, C., Alle, M., Kang, S. and Hochschild, V., 2010. Temporal and spatial aspects of snow distribution in the Nam Co Basin on the Tibetan Plateau from MODIS data. Remote Sens., 2, pp. 2700–2712.

Kumar, V. and Garg, R.D., 2012. Comparison of different mapping techniques for classifying hyperspectral data. Journal of the Indian Society of Remote Sensing, 40(3), pp.411-420.

Kumar, V., Agrawal, P. and Agrawal, S., 2017. ALOS PALSAR and Hyperion Data Fusion for Land Use Land Cover Feature Extraction. Journal of the Indian Society of Remote Sensing, 45(3), pp.407-416.

Li, X., Jiang, W., Sheng, S., Chen, Q., Sun, H., Lei, B. and Feng, J., 2009. "", MIPPR 2009 Remote Sensing and GIS Data Processing and Other Applications.

Lillesand, T.M., Kiefer, R.W. and Chipman, J.W., 1999. Remote Sensing and Image Interpretation.John Wiley & Sons, Inc, 9-10, pp. 592-597.

Mitran, T., Ravisankar, T., Fyzee, M.A., Suresh, J.R., Sujatha, G. and Sreenivas, K., 2015. Retrieval of soil physicochemical properties towards assessing salt-affected soils using Hyperspectral Data. Geocarto International, 30(6), pp.701-721.
Negi, H.S. and Kokhanovsky, A., 2011. Retrieval of snow grain size and albedo of western Himalayan snow cover using satellite data. The Cryosphere, 5(4), p.831.
Negi, H.S., Shekhar, C. and Singh, S.K., 2015. Snow and glacier investigations using hyperspectral data in the Himalaya. Current Science, 108(5), p.892.
Negi, H.S., Singh, S.K., Kulkarni, A.V. and Semwal, B.S., 2010. Field-based spectral reflectance measurements of seasonal snow cover in the Indian Himalaya. International Journal of Remote Sensing, 31(9), pp.2393-2417.
Nolin, A.W. and Dozier, J., 2000. A hyperspectral method for remotely sensing the grain size of snow. Remote sensing of Environment, 74(2), pp.207-216.
Pande, H., Tiwari, P.S. and Dobhal, S., 2009. Analyzing hyper-spectral and multi-spectral data fusion in spectral domain. Journal of the Indian Society of Remote Sensing, 37(3), pp.395-408.
Pargal, S., Agarwal, S., Gupta, P.K. and van der Werff, H.A., 2011, November. Spatial-spectral endmember extraction for spaceborne hyperspectral data. In Image Information Processing (ICIIP), 2011 International Conference on (pp. 1-6). IEEE.
Patel, H.D., Krishnamurthy, R. and Azeez, M.A., 2016. Effect of Biofertilizer on Growth, Yield and Bioactive Component of Plumbago zeylanica (Lead Wort). Journal of Agricultural Science, 8(5), p.141.
Rama Rao, N., Garg, P.K. and Ghosh, S.K., 2007. Evaluation of radiometric resolution on land use/land cover mapping in an agricultural area. International Journal of Remote Sensing, 28(2), pp.443-450.
Rekha, P.N., Gangadharan, R., Pillai, S.M., Ramanathan, G. and Panigrahi, A., 2012, December. Hyperspectral image processing to detect the soil salinity in coastal watershed. In Advanced Computing (ICoAC), 2012 Fourth International Conference on (pp. 1-5). IEEE.
Rinne, J., Aurela, M. and Manninen, T., 2009. A simple method to determine the timing of snow melt by remote sensing with application to the CO2 balances of northern mire and heath ecosystems. Remote Sens., 1, pp. 1097–1107.
Rowan, L.C. and Mars, J.C., 2003. Lithologic mapping in the Mountain Pass, California area using advanced spaceborne thermal emission and reflection radiometer (ASTER) data. Remote sensing of Environment, 84(3), pp.350-366.
Saha, A., Thakur, P.K. and Chouksey, A., 2017. Hydrological Simulation using Process Based and Empirical Models for Flood Peak Estimation‖, International Journal of Advanced Remote Sensing and GIS, 6(1), pp 2253-2266.
Silverman, E.M., 2000. Affordable carbon-carbon composite spacecraft radiator demonstration program. In Aerospace Conference Proceedings, 2000 IEEE (Vol. 4, pp. 207-214). IEEE.
Singh, M., Mishra, V.D., Thakur, N.K. and Sharma, J.D., 2015. Expansion of empirical-statistical based topographic correction algorithm for reflectance modeling on Himalayan terrain using AWiFS and MODIS sensor. Journal of the Indian Society of Remote Sensing, 43(2), pp.379-393.
Singh, D. and Singh, R., 2015. Evaluation of EO-1 Hyperion Data for Crop Studies in Part of Indo-Gangatic Plains: A Case Study of Meerut District. Advances in Remote Sensing, 4(04), p.263.
Smith, G.M. and Curran, J.P., 1998. Methods for estimating image signal-to-noise ratio (SNR). In: P.M. Atkinson and N.J. Tate (Editors), Advances in remote sensing and GIS. John Wiley and sons, Chichester, New York, Weinheim, Brisban, singapore, Toranto, pp. 61-73.
Tatsumi, K., Ohgi, N., Harada, H., Kawanishi, T., Sakuma, F., Narimatsu, Y., Inada, H., Kawashima, T. and Iwasaki, A., 2010. Onboard spectral calibration for the Japanese Hyper-spectral sensor. J]. Proc. of SPIE, 7826, p.782625.
Ustin, S. L., DiPietro, D., Olmstead, K., Underwood, E. and Scheer, G. J., 2002. Hyperspectral Remote Sensing for Invasive Species Detection and Mapping. IEEE Transactions on Geoscience and Remote Sensing, 36(4), pp. 1568–1660.
Wang, J., Li, H., Hao, X., Huang, X., Hou, J., Che, T., Dai, L., Liang, T., Huang, C., Li, H. and Tang, Z., 2014. Remote sensing for snow hydrology in China: challenges and perspectives. Journal of Applied Remote Sensing, 8(1), pp.084687-084687.
Wikipedia source- https://en.wikipedia.org/wiki/Himachal_Pradesh
Wikipedia source- https://en.wikipedia.org/wiki/Rohtang_Tunnel
Zhao, S., Jiang, T. and Wang, Z., 2013. Snow grain-size estimation using Hyperion imagery in a typical area of the Heihe River Basin, China. Remote Sensing, 5(1), pp.238-253.